

# Density distribution in the liquid-vapor interface of a dilute alloy of Pb in Ga

Meishan Zhao and Stuart A. Rice

*The James Franck Institute and Department of Chemistry, The University of Chicago, Chicago, Illinois, 60637*

(Received 7 March 2000; revised manuscript received 17 July 2000; published 5 February 2001)

This paper is concerned with the calculation of the density distribution along the normal in the liquid-vapor interface of a dilute alloy of Pb in Ga. The results of self-consistent quantum Monte Carlo simulations of that distribution are in good agreement with the experimentally inferred distribution. In particular, the simulations reproduce the finding that the excess Pb in the liquid-vapor interface forms a monolayer that is the outermost stratum of the interface. However, the 1000-atom simulation sample has a cross section of only 70 atoms, so the area of the liquid-vapor interface in these simulations is too small to permit development of long-range translational order in the Pb monolayer, and the simulations do not reproduce the experimental finding of hexagonal crystalline order in that monolayer.

DOI: 10.1103/PhysRevB.63.085409

PACS number(s): 68.03.-g

## I. INTRODUCTION

This paper describes a theoretical analysis of the density distribution along the normal in the liquid-vapor interface of a dilute Pb in Ga alloy; it is designed to complement the experimental studies of that interface reported by Yang, Li, Huang, and Rice.<sup>1</sup>

The major elements of our current theoretical understanding of the structure of the liquid-vapor interface of an alloy were obtained from the results of calculations by Gryko and Rice,<sup>2-4</sup> and by Harris, Gryko, and Rice.<sup>5,6</sup> They showed that in the liquid-vapor interface of a homovalent mixture of alkali metals there are three important structural features. These are: (i) The distribution of the total ion density along the normal to the interface (the longitudinal density distribution) is stratified for 3–4 atomic diameters into the bulk liquid. (ii) The component of the mixture that is in excess in the interface forms a pure monolayer that is the outermost layer of the liquid-vapor transition region. (iii) There is a deficiency, relative to the bulk concentration, of that component in the second layer of the stratified interface; the bulk concentration is reached in the fourth atomic layer.

Because electron density differences associated with ions of the same valence but different diameters are modest, the qualitative aspects of the structural features found in their calculations should be common to the class of homovalent alloys, irrespective of the valence. That this is so is verified by the results of grazing incidence x-ray diffraction and x-ray reflectivity studies of the liquid-vapor interface of a dilute alloy of Bi in Ga, reported by Rice and co-workers.<sup>7,8</sup> Their studies reveal that the excess Bi in the interface is concentrated in a monolayer that forms the outer layer of the interface. They also find that the Bi monolayer has the structure of a supercooled liquid, and that the stratification of the longitudinal density distribution of the underlying Ga host is sensibly the same as in pure Ga. Pershan and co-workers<sup>9</sup> have reported a similar set of studies of an alloy of In with Ga; they also conclude that the excess In concentration in the interface is concentrated in a monolayer that forms the outer layer of the interface. Calculations of the longitudinal density distributions in the BiGa and InGa alloy liquid-vapor inter-

faces, by Zhao, Chekmarev, and Rice,<sup>10,11</sup> are in good agreement with the experimental data. The calculations of the structure of the liquid-vapor interface of InGa alloys<sup>11</sup> also reveal a deficiency of In atoms in the layer just below the outermost layer, just as predicted for Cs in the binary alloy of Cs in Na.<sup>6</sup>

The electron density differences associated with ions of different valences and different diameters are usually substantial, hence there are likely to be some qualitative differences between the structures of the liquid-vapor interfaces of homovalent and heterovalent alloys. Indeed, the experimental studies of Lei, Huang, and Rice<sup>12</sup> of a dilute Sn in Ga alloy provide evidence that the atomic distribution in its liquid-vapor interface differs somewhat from the atomic distribution in the liquid-vapor interface of a dilute alloy of Bi in Ga. Specifically, unlike the atomic distribution in the liquid-vapor interface of the homovalent BiGa alloy, in the heterovalent SnGa alloy the excess Sn segregates into both the outermost and the second layers of the liquid-vapor interface; the outermost layer is pure two-dimensional liquid Sn, with an effective atomic diameter about 6% smaller than in bulk Sn at its (much higher) melting temperature, while the second layer has about 22% Sn, and there is not any detectable excess of Sn in any of the deeper layers. The source of the difference in the distributions of the surface active components in BiGa and SnGa alloys is attributed to the location of the outermost peak of the conduction electron density distribution between the first and the second ion layers in the liquid-vapor interface. As already noted, the excess Bi atoms in the liquid-vapor interface of a BiGa alloy form only one layer. Since the conduction electron density of trivalent liquid Bi is somewhat smaller than that of trivalent liquid Ga, adding Bi to the second layer of the liquid-vapor interface would decrease the conduction electron density in that layer and thereby increase the electron density gradient and the electron kinetic energy. This argument suggests that, in general, reduction of the conduction electron kinetic energy is an important factor in determining the distribution of excess concentration of a segregated component among the layers of the stratified liquid-vapor interface of an alloy.

The results of Yang, Li, Huang, and Rice,<sup>1</sup> and the pre-

liminary report of related experiments by Yang, Gidalevitz, Li, Huang, and Rice,<sup>13</sup> show that in a dilute alloy of Pb in Ga alloy, at  $T=331$  K, there is a monolayer of Pb that is the outermost layer of the liquid-vapor interface, and that there is no measurable amount of Pb in the second and deeper layers of the liquid-vapor transition region. Their data also show that below  $58^\circ\text{C}$  that Pb monolayer is an ordered hexagonally packed solid, and that there is a first order transition to a hexatic phase at about  $58^\circ\text{C}$ .

In this paper we focus attention on the calculation of the longitudinal density distribution in the liquid-vapor interface of a dilute alloy of Pb in Ga; a theoretical study of the transverse (in-the-plane) atomic distribution in the outermost layer of the liquid-vapor interface of this alloy will be described in a later paper. The separation of these analyses is made because the practical details of each are different. In particular, to calculate the longitudinal density distribution by a self-consistent quantum Monte Carlo simulation the sample must have sufficient depth to permit development of the equilibrium structure of the bulk liquid and the liquid-vapor interface. The consequence of this requirement is that the area of the liquid-vapor interface is small, indeed too small to permit satisfactory simulation of any transverse structure with long range order. On the other hand, once the longitudinal structure of the liquid-vapor interface is known, the transverse structure of the outermost layer can be simulated using a sample consisting of only a few layers. For the number of atoms that can be dealt with in our self-consistent quantum Monte Carlo simulation the number of atoms per layer can then be about 1000, which is sufficient to permit satisfactory simulation of any transverse structure with long-range order.

The results of the calculations reported in this paper provide an additional test of the methodology employed in our self-consistent quantum Monte Carlo simulations of the liquid-vapor interface of an alloy. In particular, the problem that must be addressed in simulating the properties of a heterovalent alloy is the choice of reference background for the pseudopotential calculations. The valence difference between solute and host atoms in a dilute heterovalent alloy implies that the local charge density varies substantially as different ion core positions are sampled. Given the very strong dependence of the binding energy of an atom, and of the effective interaction between atoms, on the electron density, it is not obvious that the use of a homogeneous jellium

reference distribution, such as employed in previously reported calculations, will adequately capture the interplay between the core potential and the electron density in an alloy with local variations in charge density. In fact, the results of our calculations of the longitudinal density distribution in the liquid-vapor interface of a dilute Pb in Ga alloy are in good agreement with the experimentally inferred distribution, thereby implying that the homogeneous jellium reference distribution is a reasonable first approximation.

Finally, the results of our simulations are also used to test the utility of the so called ‘‘ordering potential’’ in the description of the liquid-vapor interface of an alloy.

## II. THEORETICAL BACKGROUND

The pseudopotential theory of the liquid-vapor interface of a metal has been described in our previous papers<sup>2-6,10,11,14,22</sup> to which the reader is referred for details. We shall briefly describe only those aspects of the theoretical analysis required for comprehension of the character of the calculations carried out.

### A. Representation of the binary alloy Hamiltonian

The pseudopotential Hamiltonian has the form

$$\mathbf{H} = \sum_{i=1}^N \frac{\mathbf{p}_i^2}{2m} + \sum_{i=1}^N \sum_{j<i}^N \phi_{\text{eff}}(|\mathbf{R}_i - \mathbf{R}_j|; n_e(\mathbf{r})) + U_0[\rho_0(\mathbf{r}), n_e(\mathbf{r})], \quad (1)$$

where  $\mathbf{p}_i$  is the momentum of the  $i$ th atom with mass  $m$ ,  $\phi_{\text{eff}}(|\mathbf{R}_i - \mathbf{R}_j|; n_e(\mathbf{r}))$  is the effective pair potential between ions  $i$  and  $j$ ,  $R = |\mathbf{R}_i - \mathbf{R}_j|$  is the distance between atom  $i$  and atom  $j$ , and  $\rho_0(\mathbf{r})$  and  $n_e(\mathbf{r})$  are reference jellium and electron densities. The functional  $U_0[\rho_0(\mathbf{r}), n_e(\mathbf{r})]$  is a structure independent contribution to the energy which is, however, dependent on the electron and jellium densities. We use atomic units for all physical quantities in the following discussion, unless specified otherwise.

The structure independent energy  $U_0[\rho_0(\mathbf{r}), n_e(\mathbf{r})]$  is a functional of both the reference jellium density and the electronic density; it has the form

$$\begin{aligned} U_0[\rho_0(\mathbf{r}), n_e(\mathbf{r})] = & \frac{3(3\pi^2)^{2/3}\sigma}{10} \int_0^\infty [n_e(\mathbf{r})]^{5/3} dz + \frac{\sigma}{72} \int_0^\infty \frac{|\nabla^2 n_e(\mathbf{r})|}{n_e(\mathbf{r})} dz + \frac{\sigma}{540(3\pi^2)^{2/3}} \int_0^\infty dz [n_e(\mathbf{r})]^{2/3} \left[ \left( \frac{\nabla^2 n_e(\mathbf{r})}{n_e(\mathbf{r})} \right)^2 \right. \\ & - \frac{9}{8} \left( \frac{\nabla^2 n_e(\mathbf{r})}{n_e(\mathbf{r})} \right) \left( \frac{\nabla n_e(\mathbf{r})}{n_e(\mathbf{r})} \right)^2 + \left. \frac{1}{3} \left( \frac{\nabla n_e(\mathbf{r})}{n_e(\mathbf{r})} \right)^4 \right]^2 - 2\pi\sigma \int_0^\infty dz \int_0^\infty dz' [\rho_0(z)\rho_0(z') - n_e(z)n_e(z')] |z - z'| \\ & + 2\sigma \int_0^\infty n_e(z) \varepsilon_{xc}[n_e(z)] dz + 2\sigma \int_0^\infty \rho_0(z) \varepsilon_{ps}[n_e(z)] dz. \end{aligned} \quad (2)$$

The first three terms of this equation are, respectively, the Fermi-Thomas uniform density contribution to the kinetic energy of a liquid metal with surface area  $\sigma$ , the von Weisacker first density correction to the kinetic energy of the inhomogeneous electron gas,<sup>23</sup> and the Kirzhnits second-order gradient correction to the kinetic energy of the inhomogeneous electron gas.<sup>24</sup> The fourth term is the electrostatic energy of the system that arises from the difference between the electron and ion density distributions in the liquid-vapor transition zone, and the fifth term is the exchange-correlation contribution to the energy in the representation proposed by Vosko<sup>25</sup> with inclusion of the density gradient correction proposed by Langreth.<sup>26</sup> The last term is the electron-ion pseudopotential contribution to the electronic energy, with  $\varepsilon_{\text{ps}}[n_e(z)]$  the ionic pseudopotential (which is a function of the electron density distribution).

The major difference between the pseudopotential representations of a pure metal and a binary alloy is found to be in the structure-independent energy  $\varepsilon_{\text{ps}}[n_e(z)]$ . For a binary alloy we have<sup>3,11</sup>

$$\begin{aligned} \varepsilon_{\text{ps}} = & \frac{3}{k_F^3} \int_0^{k_F} f(q, q) q^2 dq - \frac{1}{\pi} \sum_{i=1}^2 X_i \int_0^\infty dq \{ \bar{Z}_i^2 |M_i(q)|^2 \\ & - (z_i^*)^2 F_{ii}(q) \} - \frac{2\pi}{\Omega} \sum_{i=1}^2 \sum_{j=1}^2 z_i^* z_j^* X_i X_j \lim_{q \rightarrow 0} \frac{1 - F_{ij}(q)}{q^2} \\ & + \left( \frac{\alpha}{r_s} + \frac{\beta}{r_s} \right), \end{aligned} \quad (3)$$

where  $k_F$  is the Fermi wave number,  $f(q, q)$  is the diagonal matrix element of the Fourier transform of the nonlocal bare electron-ion pseudopotential  $V_{\text{ps}}^{\text{ion}}(r)$ ,  $M_i(q)$  is the Fourier transform of the depletion hole distribution,  $X_i$  is the mole fraction of the  $i$ th component, and  $r_s$  is the radius of the sphere that has volume equal to the inverse of the valence electron density in the bulk liquid,  $n_{e, \text{bulk}}$ :

$$\frac{1}{n_{e, \text{bulk}}} = \frac{4\pi}{3} r_s^3. \quad (4)$$

The parameters  $\alpha$  and  $\beta$  in Eq. (3) were determined by imposing the requirement that the calculated and observed pressure and heat of vaporization agree with the observed values at the temperature of interest.

### B. Electron-ion pseudopotential

For the calculations reported in this paper we employed the nonlocal energy independent model pseudopotential proposed by Woo, Wang, and Matsuura.<sup>27</sup> This potential has been previously used by us<sup>10,11,14-22</sup> in studies of the structures of the liquid-vapor interfaces of several pure metals and binary alloys. It has the form

$$V_{\text{ps}}^{\text{ion}}(r) = \sum_l \{ \bar{V}_l(r) + [V_{1l}(r) - \bar{V}_l(r)] |R_{1l}\rangle \langle R_{1l}| \} |l\rangle \langle l|, \quad (5)$$

TABLE I. Ionic pseudopotential parameters (in atomic units a.u.).  $r_{\text{max}}$  is the maximum value of  $r$  in the radial wave function.

	$l$	$E_{1l}$	$R_l$	$B_{1l}$	$r_{\text{max}}$
Ga	0	1.128 60	1.941 04	1.546 51	35.0
	1	1.105 06	0.534 97	4.344 04	45.0
	2	0.472 14	2.023 58	0.335 13	55.0
Pb	0	1.554 86	2.007 22	1.997 71	35.0
	1	1.206 90	1.888 94	2.124 80	45.0
	2	0.714 19	2.662 49	1.511 53	55.0

where  $\bar{V}_l(r)$  is a pseudopotential average over all states other than the first valence state for a given angular momentum  $l$ ,  $|R_{1l}\rangle$  is the radial part of the wave function for the state  $|1l\rangle$ , and  $|l\rangle$  is a projection onto the state with angular momentum  $l$ . With these definitions the model pseudopotential takes the form

$$V_{1l}(r) = \begin{cases} -B_{1l} + Z_l/r, & r \leq R_l; \\ Z_l/r, & r > R_l, \end{cases} \quad (6)$$

where  $B_{1l}$ ,  $Z_l$ , and  $R_l$  are parameters that are usually determined by a pseudo-eigenfunction expansion and perturbation theory.  $Z$  is the valence of the ion. The averaged pseudopotential  $\bar{V}_l(r)$  is calculated in the same fashion as is  $V_{1l}(r)$  except for replacing the parameter  $B_{1l}$  with  $\bar{B}_{1l}$ . The state  $|1l\rangle$  is separated into radial and angular parts, such that

$$\langle x|1l\rangle = N \frac{1}{r} y_{1l}(r) Y_{lm}(\theta, \phi), \quad (7)$$

where  $N$  is a normalization constant,  $Y_{lm}(\theta, \phi)$  is a spherical harmonic function, and  $y_{1l}(r)$  is the radial wave function given by

$$y_{1l}(r) = \begin{cases} M_{\nu, l+1/2}(2\lambda r), & r \leq R_l; \\ W_{\nu_0, l+1/2}(2\lambda_0 r), & r > R_l, \end{cases} \quad (8)$$

where  $M_{\nu, l+1/2}(2\lambda r)$  and  $W_{\nu_0, l+1/2}(2\lambda_0 r)$  are, respectively, the regular and irregular Whittaker functions. The parameters of the Whittaker functions are

$$\lambda_0 = \sqrt{-2E_{1l}}, \quad (9)$$

$$\lambda = \sqrt{-2(E_{1l} + B_{1l})}, \quad (10)$$

$$\nu_0 = \frac{Z_l}{\sqrt{-2E_{1l}}}, \quad (11)$$

$$\nu = -\frac{Z_l}{\sqrt{-2(E_{1l} + B_{1l})}}, \quad (12)$$

with  $E_{1l}$  the spectroscopic term energy of the state  $|1l\rangle$ . Table I gives the potential parameters we have used for our study of the structure of the liquid-vapor interface of the dilute Pb in Ga alloy.

### C. Effective ion-ion pair potential

The ion-ion pair potential in the inhomogeneous liquid metal is calculated using a local density approximation and the ion-ion pair potential of the homogeneous liquid metal,

$$\phi_{\text{eff}} = \phi_H \left( R; \frac{1}{2} [n_e(\mathbf{R}_i) + n_e(\mathbf{R}_j)] \right), \quad (13)$$

where  $R = |\mathbf{R}_i - \mathbf{R}_j|$ . In a homogeneous liquid metal with valence electronic density  $n_e(\mathbf{r})$  the ion-ion pair interaction is

$$\begin{aligned} \phi_H(R) &= \frac{z_i^* z_j^*}{R} \left\{ 1 - \frac{1}{\pi} \int_0^\infty [F_{ij}(q) + F_{ji}(q)] \frac{\sin(qR)}{q} dq \right\} \\ &+ \phi_{\text{BM}}(R) + \phi_{\text{vw}}(R). \end{aligned} \quad (14)$$

The first term in Eq. (14) is due to the direct Coulomb repulsion between ions with effective valence charges  $z_i^*$  and  $z_j^*$ . The second term is an indirect interaction mediated by the conduction electrons, the so-called band structure energy. This potential term tends to offset the effect of the strong Coulomb repulsion and thus lowers the energy of the system.  $\phi_{\text{BM}}(R)$  is the Born-Mayer core-core repulsion interaction,<sup>28</sup>

$$\phi_{\text{BM}}(R) = A_{\text{BM}} e^{-B_{\text{BM}} R}, \quad (15)$$

where  $A_{\text{BM}}$  and  $B_{\text{BM}}$  are the Born-Mayer potential parameters, and  $\phi_{\text{vw}}(R)$  is the van der Waals polarization interaction between the ion cores.<sup>3</sup> In general, both  $\phi_{\text{BM}}(R)$  and  $\phi_{\text{vw}}(R)$  are much smaller than the other terms contributing to the energy of the liquid metal.

The effective valence charges  $z_i^*$  and  $z_j^*$  are defined by

$$z_i^* z_j^* = Z_i Z_j - \bar{Z}_i \bar{Z}_j \quad (16)$$

where  $Z$  is the true valence charge and  $\bar{Z}$  is the depletion hole charge that originates from the orthogonality condition between the valence and core electron wave functions.

The normalized energy wave-number characteristic function  $F_N(q)$ , as derived by Shaw,<sup>29</sup> is

$$\begin{aligned} F_{ij}(q) &= \frac{\Omega^2 q^4}{16\pi^2 z_i^* z_j^*} \left\{ \frac{[1 - \epsilon(q)](v_1 + v_2)^2}{\epsilon(q)} + 2g(q)(v_1 + v_2) \right. \\ &\left. + \epsilon(q)g(q)^2 + h(q) \right\}, \end{aligned} \quad (17)$$

where  $\Omega = (\rho_{\text{bulk}})^{-1}$  is the volume per atom,  $\rho_{\text{bulk}}$  is the bulk liquid density, and  $\epsilon(q)$  is the wave-number-dependent Hartree dielectric function. The local potential contributions  $v_1$  and  $v_2$ , arising from the valence charge  $Z$  and the depletion hole charge  $\bar{Z}$ , are given by

$$v_1 = -\frac{2\pi}{\Omega q^2} (Z_i + Z_j), \quad (18)$$

$$v_2 = -\frac{2\pi}{\Omega q^2} (\bar{Z}_i + \bar{Z}_j). \quad (19)$$

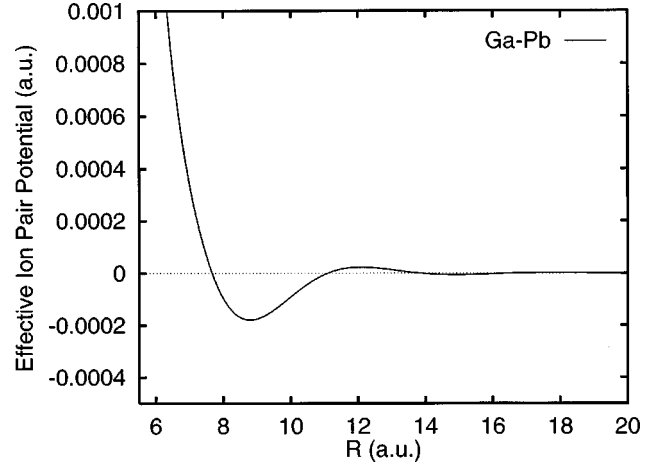


FIG. 1. The effective ion-ion pair interaction potential in liquid  $\text{Ga}_{0.86}\text{Pb}_{0.14}$  with bulk density  $0.04759 \text{ atoms}/\text{\AA}^3$ .

$g(q)$  and  $h(q)$  are, respectively, the nonlocal screening function and the nonlocal bare pseudopotential contribution to the second order approximation. They are given by

$$g(q) = \frac{4}{\pi^2 q^2 \epsilon(q)} \int_{k \leq k_F} \frac{f(\mathbf{k}, \mathbf{q})}{k^2 - |\mathbf{k} + \mathbf{q}|^2} d\mathbf{k}, \quad (20)$$

$$h(q) = \frac{4}{\pi^2 q^2} \int_{k \leq k_F} \frac{|f(\mathbf{k}, \mathbf{q})|^2}{k^2 - |\mathbf{k} + \mathbf{q}|^2} d\mathbf{k}, \quad (21)$$

with  $f(\mathbf{k}, \mathbf{q})$  the matrix elements of the Fourier transform of the nonlocal bare electron-ion pseudopotential  $V_{\text{ps}}^{\text{ion}}(r)$ . Figure 1 shows the effective GaPb pair interaction in the dilute binary alloy with density  $0.04665 \text{ atoms}/\text{\AA}^3$ .

### D. Ordering potential

Bhatia and Thornton<sup>30</sup> proposed the use of a concentration weighted effective ion-ion interaction which they and others<sup>31–35</sup> have employed to describe local order in a binary alloy. Consider the second term on the right side of Eq. (1),

$$V(R) = \sum_{i=1}^N \sum_{j<i} \phi_{\text{eff}}(|\mathbf{R}_i - \mathbf{R}_j|; n_e(\mathbf{r})). \quad (22)$$

Neglecting the short ranged Born-Mayer repulsive and van der Waals attractive interactions between the ions, the momentum space representation of the ion-ion interactions has the form

$$u_{\mu\nu}(q) = \frac{4\pi z_\mu^* z_\nu^*}{q^2} - \frac{q^2}{4\pi} \left( 1 - \frac{1}{\epsilon(q)} \right) u_\mu(q) u_\nu(q), \quad (23)$$

where  $\mu = 1, 2$ ,  $\nu = 1, 2$ . We define the concentration weighted interactions

$$u_{NN} = X_1^2 u_{11} + X_2^2 u_{22} + 2X_1 X_2 u_{12}, \quad (24)$$

$$u_{Nc} = X_1 u_{11} - X_2 u_{22} + (X_2 - X_1) u_{12}, \quad (25)$$

$$u_{cc} = u_{11} + u_{22} - 2u_{12}, \quad (26)$$

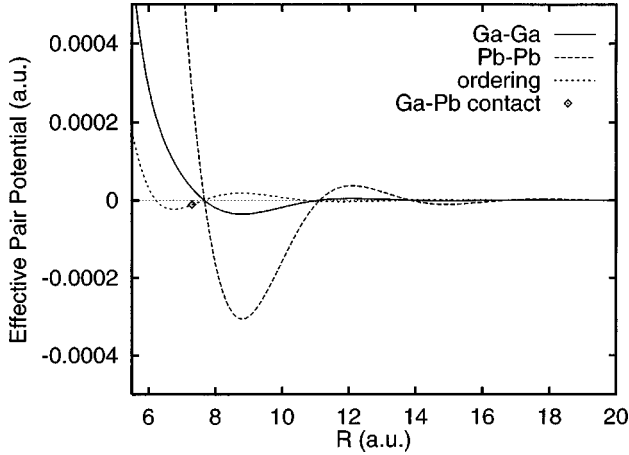


FIG. 2. The ordering potential and related ion-ion pair interaction potentials in liquid  $\text{Ga}_{0.86}\text{Pb}_{0.14}$  with bulk density  $0.04759$  atoms/ $\text{\AA}^3$ .

that can also be written

$$u_{NN} = \frac{4\pi\bar{z}^2}{q^2} - \frac{q^2}{4\pi} \left(1 - \frac{1}{\epsilon(q)}\right) \bar{u}^2(q), \quad (27)$$

$$u_{Nc} = \frac{4\pi\bar{z}\Delta z}{q^2} - \frac{q^2}{4\pi} \left(1 - \frac{1}{\epsilon(q)}\right) \bar{u}(q)\Delta u(q), \quad (28)$$

$$u_{cc} = \frac{4\pi(\Delta z)^2}{q^2} - \frac{q^2}{4\pi} \left(1 - \frac{1}{\epsilon(q)}\right) [\Delta u(q)]^2, \quad (29)$$

with

$$\bar{u}(q) = X_1 u_1(q) + X_2 u_2(q). \quad (30)$$

As before,  $X_1$  and  $X_2$  are the mole fractions of the two components of the binary alloy. In Eqs. (28) and (29),  $\Delta u = u_1 - u_2$  and  $\Delta z = z_1^* - z_2^*$ . As defined,  $u_{NN}$  has the same form as does the ion pair interaction in a pure liquid metal with effective valence  $\bar{z}$ , again neglecting the Born-Mayer repulsive and van der Waals attractive interactions between the ions. Note that  $u_{Nc}$  is a difference potential; if the difference between the effective valences of the two components in the alloy is small, the ion-ion interactions in the alloy are adequately approximated by  $u_{NN}$ . In this limit the alloy is described in the effective valence approximation. The interaction defined by Eq. (29),  $u_{cc}$ , is called the ordering potential. It is related to the so called ‘‘ordering energy’’ by

$$W = \rho_{\text{bulk}} \int u_{cc}(r) g(r) dr. \quad (31)$$

If  $W$  is negative, there is a preference for like atoms in the alloy to be close together and if  $W$  is positive there is a preference for unlike atoms to be close together. Typically,  $W$  and  $u_{cc}$  have the same sign at the separation corresponding to contact between ion cores, so the sign and magnitude of  $u_{cc}$  can be used as the signature of local composition. Figure 2 displays the ordering potential and the Ga-Ga and Pb-Pb pair potentials for the binary alloy  $\text{Ga}_{0.86}\text{Pb}_{0.14}$ . For this alloy the ordering potential is negative and much weaker

than either the Pb-Pb or the Ga-Ga interactions at the distance corresponding to PbGa contact.

### E. Character of the jellium background

A key issue that must be addressed in the pseudopotential theory of heterovalent alloys is finding an appropriate representation of the jellium background. The choice of representation is important because the jellium background defines the reference atomic density profile in the pseudoatom Hamiltonian.

When the alloy is homovalent, a uniform continuum representation of the charge density can be used, since there are only small differences between the local charge densities in the immediate neighborhoods of different ion cores of the same valence. Then the jellium distribution in the liquid-vapor interface can be represented by a simple functional form with parameters that are varied in the course of the calculation to achieve self-consistency between the electron and ion core distributions. In our previous work we used the functional form<sup>5,6,10,11</sup>

$$\rho(z, z_0, \beta) = \rho_{\text{bulk}} \left[ 1 + \exp\left(\frac{|z| - z_0}{\beta}\right) \right]^{-1} \quad (32)$$

for the charge distribution of a slab of ions with two surfaces perpendicular to the  $z$  axis. In Eq. (32),  $z_0$  is the position of the Gibbs dividing surface and  $\beta$  measures the width of the inhomogeneous region between the liquid and the vapor. This distribution is normalized by setting  $\rho_{\text{bulk}} = N/2\sigma z_0$ , where  $N$  is the total number of atoms in the slab and  $\sigma$  is the area of the slab. The parameters  $z_0$  and  $\beta$  are varied to obtain the best fit to the instantaneous ionic configuration in the simulation sample.

When the alloy is heterovalent there can be large differences between the local charge densities in the immediate neighborhoods of different ion cores with different valence. We expect that when the difference in valences of the components is large the uniform continuum representation of the charge density will not provide an adequate basis for calculation of the interactions and the self-consistent electron and ion core density profiles in the liquid-vapor interface of the alloy. However, when difference in valences of the components is small the uniform continuum approximation should be reasonably accurate. Indeed, we have shown that use of that representation for the description of the liquid-vapor interface of a dilute alloy of Sn in Ga yields good agreement with the experimentally inferred longitudinal density profile. We adopt that approximation again for the description of the liquid-vapor interface of a dilute alloy of Pb in Ga. Thus, we define the effective valence in the binary alloy to be<sup>35</sup>

$$\bar{Z} = X_1 Z_1 + X_2 Z_2. \quad (33)$$

The bulk liquid mean electron number density is then

$$n_{e,\text{bulk}} = (X_1 Z_1 + X_2 Z_2) \rho_b = \bar{Z} \rho_b, \quad (34)$$

where  $\rho_b$  is the bulk liquid atomic number density.

Our analysis of the heterovalent alloy liquid-vapor interface starts with the effective valence jellium and the reference profile displayed in Eq. (32), then calculates the electron density distribution from self-consistent solutions to the Kohn-Sham equation proposed by Eguiluz *et al.*,<sup>36,37</sup>

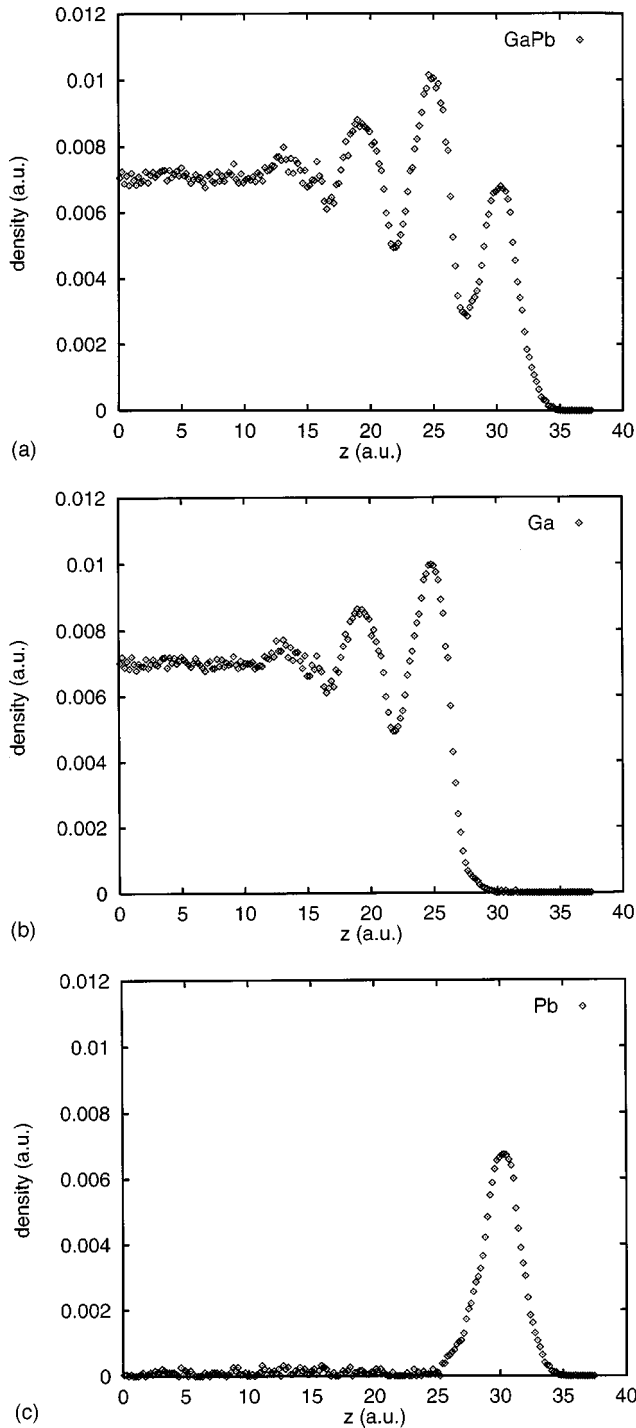


FIG. 3. Longitudinal density profiles in the liquid-vapor interface of  $\text{Ga}_{0.86}\text{Pb}_{0.14}$ ; (a) total ion density distribution; (b) Ga ion distribution; (c) Pb ion distribution.

$$\left[ -\frac{\hbar}{2m} \nabla^2 + V_{\text{eff}}(\mathbf{r}) \right] \psi_n(z) = E_n \psi_n(\mathbf{r}), \quad (35)$$

where  $V_{\text{eff}}(\mathbf{r})$  is an effective potential that includes the electron-jellium background pseudopotential interaction  $V_{\text{ps}}(\mathbf{r})$ , the exchange-correlation potential  $V_{xc}(\mathbf{r})$ , and the electrostatic potential,

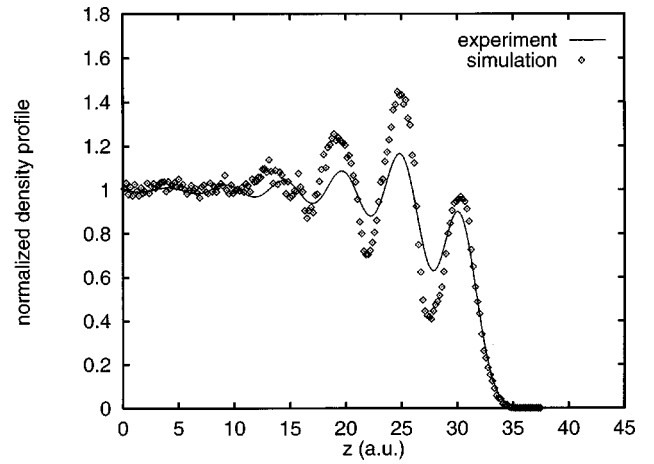


FIG. 4. Comparison of the predicted ( $\diamond \diamond \diamond$ ) and experimental (—) longitudinal density profiles in the liquid-vapor interface of a PbGa alloy (see text).

$$V_{\text{eff}}(\mathbf{r}) = V_{\text{ps}}(\mathbf{r}) + V_{xc}(\mathbf{r}) + \int d\mathbf{r}' \frac{n_e(\mathbf{r})}{|\mathbf{r} - \mathbf{r}'|}. \quad (36)$$

The exchange-correlation potential  $V_{xc}(\mathbf{r})$  is defined as the derivative

$$V_{xc}(\mathbf{r}) = \frac{\delta E_{xc}[n_e(\mathbf{r})]}{\delta n_e}, \quad (37)$$

where  $E_{xc}[n_e(\mathbf{r})]$  is the exchange and correlation energy functional, and the electron number density is calculated from

$$n_e(\mathbf{r}) = \sum_{n=1}^{\infty} f_n |\psi_n(\mathbf{r})|^2, \quad (38)$$

with  $f_n$  the electron occupation number in state  $|\psi_n(\mathbf{r})\rangle$ .

In the slab geometry of the simulation cell the ion density distributions in the  $x$  and  $y$  directions are uniform, hence the electronic wave function  $\psi_n(\mathbf{r})$  takes the form

$$\psi_n(\mathbf{r}) = e^{i(k_x x + k_y y)} \phi_n(z), \quad (39)$$

where  $k_x$  and  $k_y$  are the wave numbers in the  $x$  and  $y$  directions, respectively. The electron density is then a function only of position along the normal to the interface,  $n_e(\mathbf{r}) \equiv n_e(z)$ , and is obtained by solving the one-dimensional Kohn-Sham equation<sup>38,39</sup>

$$\left[ -\frac{\hbar}{2m} \frac{d^2}{dz^2} + V_{\text{eff}}(z; n_e(z)) \right] \phi_n(z) = \epsilon_n \phi_n(z), \quad (40)$$

$$E_n = \frac{\hbar^2}{2m_e} (k_x^2 + k_y^2) + \epsilon_n, \quad n = 1, 2, \dots \quad (41)$$

The result is

$$n_e(z) = \sum_{v=1}^{\infty} f_v |\phi_v(z)|^2, \quad (42)$$

with which we construct the electron density dependent potential  $V_{\text{eff}}(z; n_e(z))$ , and iterate the procedure until a self-consistent solution is obtained.

### III. SIMULATION METHODS AND RESULTS

All of the preceding analysis refers to the calculation of the electronic energy and the effective ion-ion interaction associated with a particular ionic configuration in the inhomogeneous liquid metal. In the system of interest the ions are mobile, and a suitable average over all allowed ionic configurations must be calculated in order to determine the longitudinal and transverse density distributions in the liquid-vapor interface. As described above, an assumed initial jellium distribution is used to generate an electronic density distribution from which the ion-electron pseudopotential and effective ion-ion interaction potentials are calculated. The initial jellium distribution is then used in a Monte Carlo simulation of the inhomogeneous liquid-vapor system. Since each Monte Carlo step changes the ion distribution, it also changes the electronic density distribution, hence the ion-electron pseudopotential and the effective ion-ion interaction; this effect is particularly important in the inhomogeneous liquid-vapor transition zone. Accordingly, when the ion distribution is changed, the electron distribution is recalculated, to be consistent with the new ion distribution; this procedure is continued until the Monte Carlo simulation converges.

The most primitive way of carrying out the program is to repeat the calculations of the effective ion-ion interaction for every move of the ions in the Monte Carlo simulation procedure. In our simulations we have adopted a more efficient computational strategy and data management scheme. Prior to starting the simulation we compute and tabulate the effective ion-ion interaction potential energies for a series of electron densities ranging from somewhat below to somewhat above the bulk density of liquid metal. During the simulation the interaction between a particular pair of ions is obtained from a rational functional interpolation for the given electron density using the precalculated data bank.

The model system for the simulations consisted of a slab of 1000 ions. The dimensions of the simulation slab were  $L_0 \times L_0 \times 2L_0$  in the  $(x, y, z)$  directions. The slab had two free surfaces in the positive  $z$  and negative  $z$  directions (normal to the two liquid-vapor interfaces), so that the area of each of the two liquid-vapor interfaces was  $\sigma = L_0^2$ . Periodic boundary conditions were applied in the  $x$  and  $y$  directions. In fact, periodic boundary conditions were also applied in the  $z$  direction, but at distances so far from the liquid-vapor interfaces that the description of those interfaces as free is valid. The size of the slab  $L_0$  was chosen such that the average density of ions in the slab matched the density of the binary alloy at the simulation temperature. The center of mass of the simulation system was located at the origin of the coordinates ( $x=0, y=0, z=0$ ). The initial ion configuration was generated by placing the particles within the boundaries of the slab, subject to the constraint that no ion-ion separation was less than the ionic diameter.

The simulations were carried out using the Metropolis

scheme<sup>40</sup> and a force bias Monte Carlo algorithm<sup>5,10</sup> to eliminate the overlaps between ion cores. The trial configurations were generated by randomly displacing a selected ion; the magnitude of the ionic displacement was chosen to lead to convergence to equilibrium with a reasonable overall acceptance ratio for the trial configurations.

As in our earlier study of the Sn in Ga liquid alloy it is instructive to make a few remarks on the composition of the simulation samples. The experimental data were obtained from studies of a dilute Pb in Ga alloy; the results obtained show that Pb completely fills the first layer of the liquid-vapor interface. To mimic the experimental macroscopic composition a double-ended simulation sample such as we have used, and containing only 1000 atoms, would have a composition  $\text{Ga}_{0.86}\text{Pb}_{0.14}$ . We have used this alloy composition in 1000 atom simulation samples at 331 K. We define a simulation pass to be 1000 ionic configurations. Using this unit, the simulations were carried out for up to 83 000 passes. The results we report here were obtained as an average over all the passes except the initial 5000.

The longitudinal density distribution of the ions was obtained from a histogram of the distance between a particle and the center of the mass of the slab; the density profiles in the and the directions were averaged to obtain the reported density distribution. We show in Fig. 3 the calculated longitudinal density profiles for  $\text{Ga}_{0.86}\text{Pb}_{0.14}$  alloy.

#### A. Comparison with experiment

The experimental studies of the liquid-vapor interface of PbGa show that the Pb which segregates in the interface is distributed as a complete monolayer atop the bulk alloy with no Pb in the second and deeper layers. A comparison of the calculated and experimental longitudinal density distributions is shown in Fig. 4 at  $T=331$  K. The agreement between the predicted and observed longitudinal density distributions is very good, but the predicted amplitude modulation of the longitudinal density distribution is somewhat greater than that observed. As in our previous study of the longitudinal density distribution<sup>10</sup> in the liquid-vapor interface of BiGa, we attribute the overshoot of the theoretical peak amplitudes to the inability of the simulation sample to support the long wavelength capillary waves which are believed to determine the temperature dependences of the amplitudes and widths of the peaks in the longitudinal density distribution.

The two surfaces of our simulation slab have about 70 atoms each, a number too small to sustain an ordered two-dimensional crystal structure. It is not surprising that the transverse pair correlation function in the liquid-vapor interface of our simulation sample is liquidlike, albeit with more pronounced and narrower peaks than in the liquid state. In this sense, our simulation fails to reproduce the experimentally observed hexagonal crystal structure of the Pb monolayer when  $T \leq 58$  °C. A better simulation of the expected behavior of a quasi two-dimensional assembly of Pb atoms will be described in a forthcoming paper.

#### ACKNOWLEDGMENTS

This work was supported by a grant from the National Science Foundation.

- <sup>1</sup>B. Yang, D. Li, Z. Huang and S. A. Rice, Phys. Rev. B **62**, 13 111 (2000).
- <sup>2</sup>M. P. D'Evelyn and S. A. Rice, Phys. Rev. Lett. **47**, 1844 (1981).
- <sup>3</sup>M. P. D'Evelyn and S. A. Rice, J. Chem. Phys. **78**, 5081 (1983).
- <sup>4</sup>M. P. D'Evelyn and S. A. Rice, J. Chem. Phys. **78**, 5225 (1983).
- <sup>5</sup>J. G. Harris, J. Gryko, and S. A. Rice, J. Chem. Phys. **87**, 3069 (1987).
- <sup>6</sup>J. G. Harris, J. Gryko, and S. A. Rice, J. Stat. Phys. **48**, 1109 (1987).
- <sup>7</sup>N. Lei, Z. Huang, and S. A. Rice, J. Chem. Phys. **104**, 4802 (1996).
- <sup>8</sup>N. Lei, Z. Huang, S. A. Rice, and C. Grayce, J. Chem. Phys. **105**, 9615 (1996).
- <sup>9</sup>M. J. Regan, P. S. Pershan, O. M. Magnussen, B. M. Ocko, M. Deutsch, and L. E. Berman, Phys. Rev. B **55**, 15 874 (1997).
- <sup>10</sup>M. Zhao, D. Chekmarev, and S. A. Rice, J. Chem. Phys. **108**, 5055 (1998).
- <sup>11</sup>S. A. Rice and M. Zhao, Phys. Rev. B **57**, 13 501 (1998).
- <sup>12</sup>N. Lei, Z. Huang, and S. A. Rice, J. Chem. Phys. **107**, 4051 (1997).
- <sup>13</sup>B. Yang, D. Gidalevitz, F. Li, Z. Huang, and S. A. Rice, Proc. Natl. Acad. Sci. U.S.A. **96**, 13 009 (1999).
- <sup>14</sup>A. Gomez and S. A. Rice, J. Chem. Phys. **101**, 8094 (1994).
- <sup>15</sup>M. Zhao, D. Chekmarev, Z. Cai, and S. A. Rice, Phys. Rev. E **56**, 7033 (1997).
- <sup>16</sup>M. Zhao, D. Chekmarev, and S. A. Rice, J. Chem. Phys. **109**, 768 (1998).
- <sup>17</sup>M. Zhao and S. A. Rice, Intern. J. Chem. **1**, URL: <http://www.ijc.com/articles/1998v1/1> (1998).
- <sup>18</sup>M. Zhao and S. A. Rice, J. Chem. Phys. **111**, 2181 (1999).
- <sup>19</sup>S. A. Rice and M. Zhao, J. Phys. Chem. A **103**, 10 159 (1999).
- <sup>20</sup>S. A. Rice, M. Zhao, and D. Chekmarev, in *Macroscopic Simulation of Interfacial Phenomena in Solids and Liquids*, Vol. 492, edited by S. R. Phillpot *et al.* (The Materials Research Society, Pittsburgh, 1998), pp. 3–14.
- <sup>21</sup>D. Chekmarev, M. Zhao, and S. A. Rice, J. Chem. Phys. **109**, 1959 (1998).
- <sup>22</sup>D. Chekmarev, M. Zhao, and S. A. Rice, Phys. Rev. E **59**, 479 (1999).
- <sup>23</sup>N. H. March, Adv. Phys. **6**, 1 (1957).
- <sup>24</sup>D. A. Kirzhnits, Zh. Eksp. Teor. Fiz. **32**, 115 (1957) [Sov. Phys. JETP **5**, 64 (1957)].
- <sup>25</sup>S. H. Vosko, L. Wilk, and M. Nusair, Can. J. Phys. **58**, 1200 (1980).
- <sup>26</sup>D. C. Langreth and M. J. Mehl, Phys. Rev. B **28**, 1809 (1983).
- <sup>27</sup>C. H. Woo, S. Wang, and M. Matsuura, J. Phys. F: Met. Phys. **5**, 1836 (1975).
- <sup>28</sup>T. L. Gilbert, J. Chem. Phys. **49**, 2640 (1968).
- <sup>29</sup>R. W. Shaw, Jr., Phys. Rev. **174**, 764 (1968).
- <sup>30</sup>A. B. Bhatia and D. E. Thornton, Phys. Rev. B **2**, 3004 (1970).
- <sup>31</sup>A. B. Bhatia and W. H. Young, Phys. Chem. Liq. **14**, 47 (1984).
- <sup>32</sup>R. N. Singh and A. B. Bhatia, J. Phys. F: Met. Phys. **14**, 2309 (1984).
- <sup>33</sup>W. H. Young, Rep. Prog. Phys. **55**, 1769 (1992).
- <sup>34</sup>Z. Jin, K. Lu, Y. Gong, and Z. Hu, J. Chem. Phys. **106**, 8830 (1997).
- <sup>35</sup>A. K. Karmakar and R. N. Joarder, Physica B **245**, 81 (1998).
- <sup>36</sup>A. G. Eguliz, D. A. Campbell, A. A. Maradudin, and R. F. Wallis, Phys. Rev. B **30**, 5449 (1984).
- <sup>37</sup>J. P. Perdew, M. Ernerhof, A. Zupan, and K. Burke, J. Chem. Phys. **108**, 1522 (1998).
- <sup>38</sup>W. Kohn and L. J. Sham, Phys. Rev. A **140**, 1133 (1965).
- <sup>39</sup>P. Hohenberg and W. Kohn, Phys. Rev. B **136**, 864 (1964).
- <sup>40</sup>N. Metropolis, A. W. Rosenbluth, M. N. Rosenbluth, A. M. Teller, and E. Teller, J. Chem. Phys. **21**, 1087 (1953).